

Rear-surface integral method for calculating thermal diffusivity: finite pulse time correction and two-layer samples

Elliot J. Carr^a, Christyn J. Wood^a

^a*School of Mathematical Sciences, Queensland University of Technology (QUT), Brisbane, Australia.*

Abstract

We study methods for calculating the thermal diffusivity of solids from laser flash experiments. This experiment involves subjecting the front surface of a small sample of the material to a heat pulse and recording the resulting temperature rise on the opposite (rear) surface. Recently, a new method was developed for calculating the thermal diffusivity from the rear-surface temperature rise, which was shown to produce improved estimates compared with the commonly used half-time approach. This new so-called *rear-surface integral method* produced a new formula for calculating the thermal diffusivity of homogeneous samples under the assumption that the heat pulse is instantaneously absorbed uniformly into a thin layer at the front surface. In this paper, we show how the rear-surface integral method can be applied to a more physically realistic heat flow model involving the actual heat pulse shape from the laser flash experiment. New thermal diffusivity formulas are derived for handling arbitrary pulse shapes for either a homogeneous sample or a heterogeneous sample comprising two layers of different materials. Presented numerical experiments confirm the accuracy of the new formulas and demonstrate how they can be applied to the kinds of experimental data arising from the laser flash experiment.

Keywords: laser flash method; thermal diffusivity; parameter estimation; heat transfer.

1. Introduction

The most popular technique for measuring the thermal diffusivity of a solid material is the laser flash method [1–3]. Originally developed by Parker et al. [4], this method involves subjecting the front surface of a small sample of the material to a heat pulse of radiant energy and recording the resulting temperature rise on the opposite (rear) surface of the sample (Figure 1). The thermal diffusivity is then calculated from the rear-surface temperature rise curve by developing a mathematical model describing the heat flow emanating from the front surface and analysing the solution of this model at the rear surface.

Parker et al. [4] assumed the sample is homogeneous and thermally insulated; the heat pulse is instantaneously and uniformly absorbed by a thin layer at the front surface; and the heat flow is one-dimensional in the direction of the thickness of the sample extending from the front surface to the rear surface (Figure 1b). These simplifying assumptions yield the now famous and widely-used formula [5–8] for the thermal diffusivity

$$\alpha \approx \frac{1.37L^2}{\pi^2 t_{0.5}}, \quad (1)$$

where L is the thickness of the sample and $t_{0.5}$ is the half-rise time, the time required for the rear-surface tempera-

ture rise to reach one half of its maximum (steady-state) value T_∞ (Figure 1d).

Since 1961, many papers have presented advances and extensions on Parker et al.’s original method. In particular, numerous papers have focussed on the *finite pulse-time effect*, that is, the observation that the heat pulse occurs over a finite duration [9, 10] and is rarely well approximated by an ideal instantaneous pulse (as assumed by Parker et al. [4]). In the one-dimensional case, the boundary condition imposing thermal insulation at the front surface [4, 11] is replaced by a boundary condition specifying the heat flux applied at the front surface based on the actual shape of the heat pulse [9] (Figure 1a). Commonly, simple functions are used to represent the pulse shape such as those describing rectangular [12], triangular [9, 12] and exponential [13] pulses. For the half-rise time approach, accounting for the finite-pulse time leads to small corrections [9, 12] to the formula for the thermal diffusivity (1).

Considerable research activity has also focussed on the application of the laser flash method to layered samples consisting of two or more adjacent homogeneous layers with distinct thermal diffusivities [13–16]. For a two layer sample, only one of the thermal diffusivities can be calculated from the temperature rise recorded at the rear surface [15, 17]. In this case, assuming the thermal diffusivity of one of the layers is known, extension of the half-rise time approach yields a formula for the thermal diffusivity of the other layer involving the half-rise time and the volumetric

Email address: elliott.carr@qut.edu.au (Elliot J. Carr)

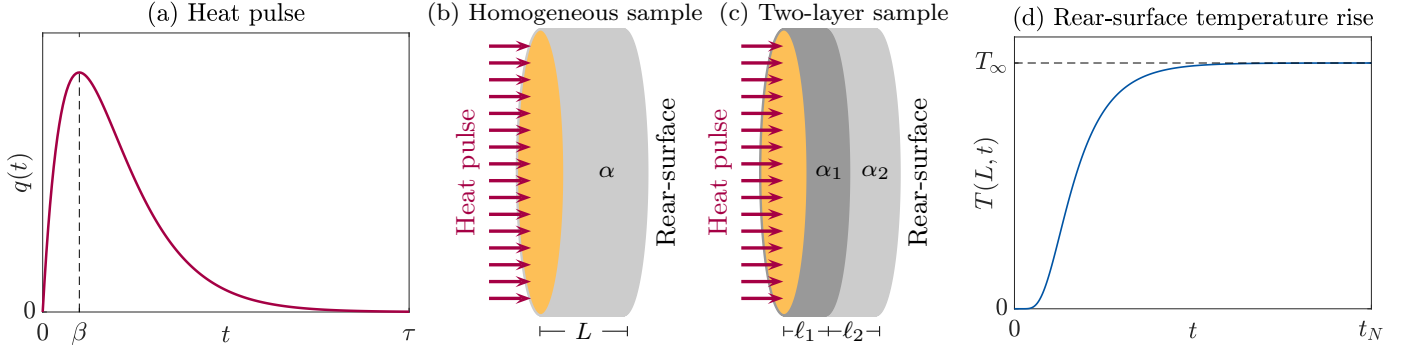


Figure 1: Schematic representation of the laser flash experiment for (b) a homogeneous sample with thickness L and thermal diffusivity α and (c) a two-layer sample consisting of two homogeneous layers of thickness ℓ_1 and ℓ_2 and thermal diffusivities α_1 and α_2 . A heat pulse of radiant energy is applied to the front surface (a) resulting in the temperature on the opposite (rear surface) of the sample rising over time (d). Eventually the temperature rise tends to a finite steady-state value, T_∞ , under the assumption of a thermally insulated sample.

heat capacity of both layers [13].

Recently, Carr [11] presented a new method for calculating the thermal diffusivity from the rear-surface temperature rise history. This so-called *rear-surface integral method* expresses the thermal diffusivity exactly in terms of the area between the theoretical rear-surface temperature rise curve, $T(L, t)$, and the steady-state temperature, T_∞ , over time (see Figure 1d). For a homogeneous and thermally insulated sample, where the heat pulse is instantaneously and uniformly absorbed by a thin layer of thickness ℓ at the front surface, the thermal diffusivity formula is given by [11]:

$$\alpha = \frac{T_\infty(L^2 - \ell^2)}{6 \int_0^\infty [T_\infty - T(L, t)] dt}. \quad (2)$$

Numerical experiments carried out on synthetic data generated by adding Gaussian noise to the theoretical rear-surface temperature rise curve, $T(L, t)$, demonstrated that the new formula (2) produces estimates of the thermal diffusivity that are more accurate than the standard formula (1).

Carr [11] essentially provided a proof-of-concept for the rear-surface integral approach applied to the classical heat flow model of the laser flash experiment [4]. In the current paper, we present two key contributions. Firstly, we extend the rear-surface integral approach to account for finite pulse time effects deriving new formulas for the thermal diffusivity for rectangular, triangular, exponential and arbitrary pulse shapes (Section 2). Secondly, we extend these new theoretical results to two layer samples, developing new formulas for the thermal diffusivity of both layers (Section 3). After deriving the new formulas, we verify their accuracy and demonstrate their application to the types of experimental data that arise from the laser flash experiment (Section 4). We then conclude with a summary of the work and a discussion regarding the limitations of the new formulas (Section 5).

2. Homogeneous sample

2.1. Heat flow model

Consider a thermally insulated homogeneous sample of uniform thickness L , thermal conductivity k , volumetric heat capacity ρc and thermal diffusivity $\alpha = k/(\rho c)$ (Figure 1b). Let $\mathcal{T}(x, t)$ be the temperature of the sample at location $0 \leq x \leq L$ and time $t \geq 0$ and assume the heat pulse applied at the front surface, $x = 0$, is initiated at $t = 0$. We assume the temperature rise, $T(x, t) = \mathcal{T}(x, t) - T_0$, above the initial uniform temperature of the sample, T_0 , resulting from the heat pulse satisfies the following heat flow model [2, 9, 12]:

$$\frac{\partial T}{\partial t}(x, t) = \alpha \frac{\partial^2 T}{\partial x^2}(x, t), \quad 0 < x < L, \quad t > 0, \quad (3)$$

$$T(x, 0) = 0, \quad 0 < x < L, \quad (4)$$

$$-k \frac{\partial T}{\partial x}(0, t) = q(t), \quad \frac{\partial T}{\partial x}(L, t) = 0, \quad (5)$$

where $q(t)$ is the heat flux function representing the laser pulse applied at the front surface of the sample (Figure 1a). Provided $\lim_{t \rightarrow \infty} q(t) = 0$ and the total amount of heat absorbed at the front surface

$$Q_\infty = \int_0^\infty q(s) ds < \infty, \quad (6)$$

the steady-state temperature rise is given by [9]:

$$T_\infty = \lim_{t \rightarrow \infty} T(x, t) = \frac{Q_\infty}{\rho c L}, \quad 0 < x < L. \quad (7)$$

This result is derived by first applying the thermally insulated boundary conditions (5) that arise in the limit $t \rightarrow \infty$ to the linear steady-state solution of the heat equation (3) yielding $\lim_{t \rightarrow \infty} T(x, t) = T_\infty$, where T_∞ is a constant. The value of T_∞ is then identified by noting that the change in the amount of heat in the sample must be balanced by the amount of heat entering through the front surface:

$$\rho c \int_0^L T(x, t) dx = Q(t), \quad (8)$$

where

$$Q(t) = \int_0^t q(s) ds. \quad (9)$$

At steady state, Eq (8) reduces to $\rho c L T_\infty = Q_\infty$ yielding the stated result (7).

2.2. Thermal diffusivity

We now extend the rear-surface integral method for calculating thermal diffusivity [11] to non-instantaneous heat pulse durations. The aim of this method is to derive a formula for the thermal diffusivity, α , in terms of an integral involving $T(L, t)$, the rear-surface temperature rise extracted from the heat flow model (3)–(5). The starting point for the derivation is the function:

$$u(x) = \int_0^\infty [T_\infty - T(x, t)] dt. \quad (10)$$

Differentiating $u(x)$ twice with respect to x , noting T_∞ (7) is a constant and using the heat equation (3) and initial condition (4) yields the differential equation [11]:

$$\frac{d^2 u}{dx^2} = -\frac{T_\infty}{\alpha}, \quad 0 < x < L, \quad (11)$$

which identifies $u(x)$ as a quadratic function:

$$u(x) = c_0 + c_1 x - \frac{T_\infty x^2}{2\alpha}. \quad (12)$$

To identify the integration constants, c_0 and c_1 , we combine the form of du/dx with the boundary conditions (5) [11] yielding:

$$\frac{du}{dx}(0) = \int_0^\infty -\frac{\partial T}{\partial x}(0, t) dt = \int_0^\infty \frac{q(t)}{k} dt = \frac{Q_\infty}{k}, \quad (13)$$

$$\frac{du}{dx}(L) = \int_0^\infty -\frac{\partial T}{\partial x}(L, t) dt = \int_0^\infty 0 dt = 0. \quad (14)$$

Imposing both of these boundary conditions on $u(x)$ (12) yields the same result, namely $c_1 = T_\infty L/\alpha$, after noting the relationship between T_∞ and Q_∞ (7). Therefore, to uniquely identify $u(x)$ we require an auxiliary condition analogous to the one required for the steady-state solution (8). Integrating $u(x)$ (10) from $x = 0$ to $x = L$, multiplying by the volumetric heat capacity ρc and reversing the order of integration yields the appropriate condition:

$$\rho c \int_0^L u(x) dx = \int_0^\infty [Q_\infty - Q(t)] dt. \quad (15)$$

Imposing this auxiliary condition on $u(x)$ (12) uniquely identifies c_0 and hence $u(x)$:

$$u(x) = \frac{\int_0^\infty [Q_\infty - Q(t)] dt}{\rho c L} + \frac{T_\infty L}{\alpha} \left[x - \frac{L}{3} - \frac{x^2}{2L} \right]. \quad (16)$$

In summary, we have derived a closed-form expression for the integral (10) by formulating and solving the boundary value problem consisting of Eqs (11) and (13)–(15).

Equating both expressions for $u(x)$, Eqs (10) and (16), at the rear surface, $x = L$, and rearranging yields a formula for the thermal diffusivity that can be expressed as:

$$\alpha = \frac{L^2}{6(I_T - I_q)}, \quad (17)$$

where

$$I_T = \int_0^\infty [1 - T(L, t)/T_\infty] dt, \quad (18)$$

$$I_q = \int_0^\infty [1 - Q(t)/Q_\infty] dt. \quad (19)$$

Eqs (17)–(19) express the thermal diffusivity explicitly in terms of L , the thickness of the sample, $T(L, t)$, the rear-surface temperature rise history, T_∞ , the steady-state temperature rise value (7), Q_∞ , the total amount of heat absorbed through the front surface (6), and $Q(t)$, the amount of heat that has been absorbed through the front surface at time t (9). For the types of functions commonly used to represent the shape of the heat pulse, which specify the finite pulse time τ , and/or peak of the pulse β (Figure 1a), the formula for the thermal diffusivity (17)–(19) simplifies significantly:

Rectangular pulse [12]:

$$q(t) = \begin{cases} \frac{Q_\infty}{\tau}, & 0 < t \leq \tau, \\ 0, & \text{otherwise,} \end{cases} \quad I_q = \frac{\tau}{2}, \quad (20a)$$

$$\alpha = \frac{L^2}{6(I_T - \frac{\tau}{2})}. \quad (20b)$$

Triangular pulse [9, 12]:

$$q(t) = \begin{cases} \frac{2Q_\infty t}{\tau\beta}, & 0 < t \leq \beta, \\ \frac{2Q_\infty(\tau - t)}{\tau(\tau - \beta)}, & \beta \leq t \leq \tau, \\ 0, & \text{otherwise,} \end{cases} \quad I_q = \frac{\tau + \beta}{3}, \quad (21a)$$

$$\alpha = \frac{L^2}{6(I_T - \frac{\tau + \beta}{3})}. \quad (21b)$$

Exponential pulse [13]:

$$q(t) = \begin{cases} \frac{Q_\infty t}{\beta^2} e^{-t/\beta}, & t > 0, \\ 0, & \text{otherwise,} \end{cases} \quad I_q = 2\beta, \quad (22a)$$

$$\alpha = \frac{L^2}{6(I_T - 2\beta)}. \quad (22b)$$

In the limit $\tau \rightarrow 0$, the rectangular pulse tends to the instantaneous pulse $q(t) = Q_\infty \delta(t)$, where $\delta(t)$ is the Dirac delta function, yielding $\alpha = L^2/(6I_T)$ as derived previously [11]. Hence, the above formulas provide simple finite pulse time corrections to the thermal diffusivity involving the duration and peak of the pulse. Application of the thermal diffusivity formula (17)–(19) to arbitrary pulse shapes is addressed later in Section 4.2.

3. Two layer sample

3.1. Heat flow model

We now consider a two-layer sample comprised of two homogeneous materials with constant but different thermodynamic properties. The first layer has thickness ℓ_1 and extends from the front surface of the sample at $x = 0$ to the interface between the two layers at $x = \ell_1$ while the second layer has thickness ℓ_2 and extends from the interface at $x = \ell_1$ to the rear surface of the sample at $x = \ell_1 + \ell_2 =: L$ (Figure 1c). The first layer is assumed to have thermal conductivity k_1 , volumetric heat capacity $\rho_1 c_1$ and thermal diffusivity $\alpha_1 = k_1/(\rho_1 c_1)$ while the second layer has thermal conductivity k_2 , volumetric heat capacity $\rho_2 c_2$ and thermal diffusivity $\alpha_2 = k_2/(\rho_2 c_2)$. Let $T_1(x, t)$ be the temperature of the sample in the first layer at location $0 \leq x \leq \ell_1$ and time $t \geq 0$ and $T_2(x, t)$ be the temperature of the sample in the second layer at location $\ell_1 \leq x \leq L$ and time $t \geq 0$. We assume the temperature rise in the first and second layers, $T_1(x, t) = \mathcal{T}_1(x, t) - T_0$ and $T_2(x, t) = \mathcal{T}_2(x, t) - T_0$, after initiation of the heat pulse at $t = 0$, satisfies the following heat flow model [13, 15]:

$$\frac{\partial T_1}{\partial t}(x, t) = \alpha_1 \frac{\partial^2 T_1}{\partial x^2}(x, t), \quad 0 < x < \ell_1, \quad t > 0, \quad (23)$$

$$\frac{\partial T_2}{\partial t}(x, t) = \alpha_2 \frac{\partial^2 T_2}{\partial x^2}(x, t), \quad \ell_1 < x < L, \quad t > 0, \quad (24)$$

$$T_1(x, 0) = 0, \quad 0 < x < \ell_1, \quad (25)$$

$$T_2(x, 0) = 0, \quad \ell_1 < x < L, \quad (26)$$

$$-k_1 \frac{\partial T_1}{\partial x}(0, t) = q(t), \quad t > 0, \quad (27)$$

$$\frac{\partial T_2}{\partial x}(L, t) = 0, \quad t > 0, \quad (28)$$

$$T_1(\ell_1, t) = T_2(\ell_1, t), \quad t > 0, \quad (29)$$

$$k_1 \frac{\partial T_1}{\partial x}(\ell_1, t) = k_2 \frac{\partial T_2}{\partial x}(\ell_1, t), \quad t > 0, \quad (30)$$

where the internal boundary conditions (29)–(30) specify continuity of temperature and heat flux at the interface between the two layers.

In a similar manner to the homogeneous case, provided $\lim_{t \rightarrow \infty} q(t) = 0$ and the total amount of heat Q_∞ absorbed at the front surface (6) is finite, the steady-state solution of the two-layer heat flow model (23)–(30) is given by [13, 18]:

$$T_\infty = \lim_{t \rightarrow \infty} T_1(x, t) = \lim_{t \rightarrow \infty} T_2(x, t) = \frac{Q_\infty}{\rho_1 c_1 \ell_1 + \rho_2 c_2 \ell_2}. \quad (31)$$

This result is derived by applying the interface conditions (29)–(30) and the thermally insulated boundary conditions (27)–(28) that arise in the limit $t \rightarrow \infty$ to the linear steady-state solutions of the heat equations (23)–(24) yielding $\lim_{t \rightarrow \infty} T_1(x, t) = \lim_{t \rightarrow \infty} T_2(x, t) = T_\infty$, where T_∞ is a constant. As with the homogeneous case, the value of T_∞ can be identified by noting that the change in the amount of heat in the sample must be balanced by the amount of heat entering the sample through the front surface:

$$\rho_1 c_1 \int_0^{\ell_1} T_1(x, t) dx + \rho_2 c_2 \int_{\ell_1}^L T_2(x, t) dx = Q(t), \quad (32)$$

where $Q(t)$ is as defined previously (9). At steady state this heat conservation statement reduces to $T_\infty [\rho_1 c_1 \ell_1 + \rho_2 c_2 \ell_2] = Q_\infty$ yielding the stated result (31).

3.2. Thermal diffusivity

We now extend the analysis of Section 2.2 to two-layer samples. The aim is again to derive a formula for the thermal diffusivity in terms of an integral involving the theoretical rear-surface temperature rise history, which for the two-layer heat flow model (23)–(30) is represented by $T_2(L, t)$. For the two-layer case, we have separate definitions of Eq (10) in each layer:

$$u_1(x) = \int_0^\infty [T_\infty - T_1(x, t)] dt, \quad (33)$$

$$u_2(x) = \int_0^\infty [T_\infty - T_2(x, t)] dt. \quad (34)$$

Using an identical procedure to the one carried out for the single-layer case yields the following differential equations and boundary conditions:

$$\frac{d^2 u_1}{dx^2} = -\frac{T_\infty}{\alpha_1}, \quad 0 < x < \ell_1, \quad (35)$$

$$\frac{d^2 u_2}{dx^2} = -\frac{T_\infty}{\alpha_2}, \quad \ell_1 < x < L, \quad (36)$$

$$\frac{du_1}{dx}(0) = \frac{Q_\infty}{k_1}, \quad \frac{du_2}{dx}(L) = 0. \quad (37)$$

The solution of Eqs (35)–(37) is

$$u_1(x) = a_0 + \frac{T_\infty(\rho_1 c_1 \ell_1 + \rho_2 c_2 \ell_2)x}{\alpha_1 \rho_1 c_1} - \frac{T_\infty x^2}{2\alpha_1}, \quad (38)$$

$$u_2(x) = b_0 + \frac{T_\infty(\ell_1 + \ell_2)x}{\alpha_2} - \frac{T_\infty x^2}{2\alpha_2}, \quad (39)$$

where a_0 and b_0 are arbitrary constants. The appropriate interface conditions are given by

$$u_1(\ell_1) = u_2(\ell_1), \quad (40)$$

$$k_1 \frac{du_1}{dx}(\ell_1) = k_2 \frac{du_2}{dx}(\ell_1), \quad (41)$$

which are derived by combining the interface conditions of the heat flow model (29)–(30) with the definitions of $u_1(x)$ and $u_2(x)$ (33)–(34). For example, the second interface condition (41) is derived as follows:

$$\begin{aligned} k_1 \frac{du_1}{dx}(\ell_1) &= \int_0^\infty -k_1 \frac{\partial T_1}{\partial x}(\ell_1, t) dt \\ &= \int_0^\infty -k_2 \frac{\partial T_2}{\partial x}(\ell_1, t) dt = k_2 \frac{du_2}{dx}(\ell_1). \end{aligned}$$

Both $u_1(x)$ and $u_2(x)$ (38)–(39) already satisfy flux continuity at the interface (41) and therefore this interface condition yields no information about a_0 and b_0 . As with the single-layer case, an additional condition is required

to completely identify the solution. The analogue of the auxiliary condition (15) for the two-layer case is:

$$\begin{aligned} \rho_1 c_1 \int_0^{\ell_1} u_1(x) dx + \rho_2 c_2 \int_{\ell_1}^L u_2(x) dx \\ = \int_0^\infty [Q_\infty - Q(t)] dt, \end{aligned} \quad (42)$$

which is derived by substituting the definitions of $u_1(x)$ and $u_2(x)$ (33)–(34) into the left-hand side of Eq (42), reversing the order of integration, combining the integrals and making use of the expression for T_∞ (31) and the heat conservation statement (32). Applying the auxiliary equation (42) and the first interface condition (40), produces a pair of linear equations that allow a_0 and b_0 to be identified. This determines the final forms for $u_1(x)$ and $u_2(x)$, which together comprise the solution to the boundary value problem consisting of Eqs (35)–(37) and (40)–(42). Since we are only interested in the rear-surface behaviour, we give only the final expression for $u_2(x)$:

$$\begin{aligned} u_2(x) = & \frac{\int_0^\infty [Q_\infty - Q(t)] dt}{\rho_1 c_1 \ell_1 + \rho_2 c_2 \ell_2} - \frac{\ell_1^2 [2T_\infty \rho_1 c_1 \ell_1 - 3Q_\infty]}{6\alpha_1 (\rho_1 c_1 \ell_1 + \rho_2 c_2 \ell_2)} \\ & - \frac{\rho_1 c_1 \ell_1^2 T_\infty [\ell_1 + 2\ell_2]}{2\alpha_2 (\rho_1 c_1 \ell_1 + \rho_2 c_2 \ell_2)} \\ & - \frac{\rho_2 c_2 T_\infty [2(\ell_1 + \ell_2)^3 - \ell_1^2 (2\ell_1 + 3\ell_2)]}{6\alpha_2 (\rho_1 c_1 \ell_1 + \rho_2 c_2 \ell_2)} \\ & + \frac{T_\infty (\ell_1 + \ell_2)x}{\alpha_2} - \frac{T_\infty x^2}{2\alpha_2}. \end{aligned} \quad (43)$$

Equating both expressions for $u_2(x)$, Eqs (34) and (43), at the rear surface, $x = L$, and rearranging yields formulas for the thermal diffusivity in either the first or second layers:

$$\alpha_1 = \frac{\ell_1^2 (\ell_1 \rho_1 c_1 + 3\ell_2 \rho_2 c_2) \alpha_2}{6\alpha_2 (\rho_1 c_1 \ell_1 + \rho_2 c_2 \ell_2) (I_T - I_q) - \ell_2^2 (3\ell_1 \rho_1 c_1 + \ell_2 \rho_2 c_2)}, \quad (44)$$

$$\alpha_2 = \frac{\ell_2^2 (3\ell_1 \rho_1 c_1 + \ell_2 \rho_2 c_2) \alpha_1}{6\alpha_1 (\rho_1 c_1 \ell_1 + \rho_2 c_2 \ell_2) (I_T - I_q) - \ell_1^2 (\ell_1 \rho_1 c_1 + 3\ell_2 \rho_2 c_2)}, \quad (45)$$

where

$$I_T = \int_0^\infty [1 - T_2(L, t)/T_\infty] dt, \quad (46)$$

$$I_q \text{ is as defined in Eq (19)}. \quad (47)$$

Both formulas (44)–(45) assume the layer thicknesses, ℓ_1 and ℓ_2 , and the volumetric heat capacities, $\rho_1 c_1$ and $\rho_2 c_2$, are known, expressing the thermal diffusivity explicitly in terms of $T_2(L, t)$, the rear-surface temperature rise history, T_∞ the steady-state temperature rise value (31), Q_∞ the total amount of heat absorbed through the front surface (6), and $Q(t)$ the amount of heat that has been absorbed through the front surface at time t (9). Calculating the thermal diffusivity of either layer also requires the thermal diffusivity of the other layer to be known, which is consistent with the well-known result that only one thermal

diffusivity of a two-layer sample can be calculated using the rear-surface temperature [15, 17]. Since the formula for I_q is identical for the homogeneous and two-layer case, the two-layer thermal diffusivity formulas for the rectangular, triangular and exponential pulses, analogous to Eqs (20)–(22), are easily obtained by substituting the expressions for I_q from Eqs (20)–(22) into Eqs (44)–(45). Finally, we confirm that removing the heterogeneity by setting $\alpha_1 = \alpha_2 = \alpha$, $\rho_1 c_1 = \rho_2 c_2 = \rho c$ and $T_2(L, t) = T(L, t)$ in both formulas (44)–(45) and rearranging for α yields the single-layer formula (17) as expected.

4. Numerical experiments

4.1. Verification of formulas

We now verify the thermal diffusivity formulas derived in Sections 2.2 and 3.2 for the homogeneous and two-layer samples. In practice, the rear-surface temperature rise history takes the form of discrete values: $\tilde{T}_0, \dots, \tilde{T}_N$, where \tilde{T}_i is the sampled value at $t_i = i\Delta t$, $\Delta t = t_N/N$ and t_N is the final sampled time. In the discrete case, provided t_N is large enough (see, e.g. [19, 20], for how to estimate steady state times), the integral I_T appearing in the thermal diffusivity formulas, Eqs (17)–(19) and (44)–(47), can be approximated using the trapezoidal rule [11]. For example, for the homogeneous sample:

$$\begin{aligned} I_T & \approx \int_0^{t_N} [1 - T(L, t)/T_\infty] dt, \\ & \approx \Delta t \sum_{i=1}^N \left(1 - \frac{\tilde{T}_{i-1} + \tilde{T}_i}{2T_\infty} \right). \end{aligned} \quad (48)$$

Verification is carried out using synthetic rear-surface temperature rise data generated from solving the heat flow model using a known set of parameter values (Table 1) given previously by Czél et al. [2]. Both the homogeneous model (3)–(5) and two-layer model (23)–(30) are solved numerically using finite volume schemes consisting of n nodes, as outlined in Appendix A and Appendix B, respectively. These numerical solutions produce sampled values of the rear-surface temperature rise at equally-spaced discrete times such that the i th sampled value \tilde{T}_i is given by $T_n(t_i)$, where T_n represents the temperature rise value in the finite volume scheme at the node located at the rear surface ($x = L$, n th node). Each estimate of the thermal diffusivity is compared to the target value in Table 1 by calculating the signed relative errors $\varepsilon = (\alpha - \tilde{\alpha})/\alpha$ (homogeneous) and $\varepsilon_k = (\alpha_k - \tilde{\alpha}_k)/\alpha_k$ for $k = 1, 2$ (two-layer) with the tilde used to indicate the estimated value produced from the rear-surface integral method.

In Table 2, results for both the homogeneous and two-layer samples are presented for the rectangular (20), triangular (21) and exponential (22) pulses with $\tau = 0.005$ s, $\beta = 0.001$ s, $Q_\infty = 7000$ J m⁻², $N = 1000$ temperature rise values, $\Delta t = 10^{-4}$ s, $t_N = 0.1$ s and $n = 500$ nodes. In all cases, the estimate agrees with the target values of the

| | | | |
|--|--|--|--|
| <i>Homogeneous (Single-layer)</i> | | | |
| $k = 222 \text{ W m}^{-1}\text{K}^{-1}, \quad \rho = 2700 \text{ kg m}^{-3}, \quad c = 896 \text{ J kg}^{-1}\text{K}^{-1}, \quad L = 0.002 \text{ m},$ | | | |
| Target value: $\alpha = k/(\rho c) = 9.1766 \times 10^{-5} \text{ m}^2\text{s}^{-1}.$ | | | |
| <i>Two-layer</i> | | | |
| $k_1 = 222 \text{ W m}^{-1}\text{K}^{-1}, \quad \rho_1 = 2700 \text{ kg m}^{-3}, \quad c_1 = 896 \text{ J kg}^{-1}\text{K}^{-1}, \quad \ell_1 = 0.00176 \text{ m},$ | | | |
| $k_2 = 16.3 \text{ W m}^{-1}\text{K}^{-1}, \quad \rho_2 = 7810 \text{ kg m}^{-3}, \quad c_2 = 480 \text{ J kg}^{-1}\text{K}^{-1}, \quad \ell_2 = 0.00024 \text{ m},$ | | | |
| Target value: $\alpha_1 = k_1/(\rho_1 c_1) = 9.1766 \times 10^{-5} \text{ m}^2\text{s}^{-1},$ | | | |
| Target value: $\alpha_2 = k_2/(\rho_2 c_2) = 4.3481 \times 10^{-6} \text{ m}^2\text{s}^{-1}.$ | | | |

Table 1: Heat flow parameter values used in all numerical experiments. In each case, the target value of the thermal diffusivity is displayed rounded to five significant figures.

| | Rectangular | Triangular | Exponential |
|--------------------|-------------------------|-------------------------|-------------------------|
| Homogeneous | | | |
| $\tilde{\alpha}$ | 9.1766×10^{-5} | 9.1766×10^{-5} | 9.1766×10^{-5} |
| ε | 2.0077×10^{-4} | 2.0078×10^{-4} | 2.0078×10^{-4} |
| Two layer | | | |
| $\tilde{\alpha}_1$ | 9.1766×10^{-5} | 9.1766×10^{-5} | 9.1766×10^{-5} |
| ε_1 | 1.5619×10^{-4} | 1.8399×10^{-4} | 1.8065×10^{-4} |
| $\tilde{\alpha}_2$ | 4.3480×10^{-6} | 4.3480×10^{-6} | 4.3480×10^{-6} |
| ε_2 | 2.0250×10^{-4} | 2.3855×10^{-4} | 2.3421×10^{-4} |

Table 2: Thermal diffusivity estimates, $\tilde{\alpha}$, $\tilde{\alpha}_1$ and $\tilde{\alpha}_2$, and corresponding signed relative errors, ε , ε_1 and ε_2 , obtained from applying the formulas (17)–(19) and (44)–(47) to the parameter values in Table 1 and the synthetic rear-surface temperature rise history discussed in Section 4.1. Results are given for the rectangular, triangular and exponential pulses given in Eqs (20)–(22).

thermal diffusivity in Table 1 to 4–5 significant digits with a relative error of approximately 10^{-4} . These small non-zero values are explained by the error present in the numerical experiment incurred from truncating the infinite upper limit of the integral I_T at the finite value t_N and approximating the resulting integral numerically (48) as well as numerically solving the heat flow models to generate the sampled values. In summary, the results in Table 2 confirm the correctness of the analysis in Sections 2.2 and 3.2.

4.2. Application to noisy data

We now investigate the accuracy of the thermal diffusivity formulas when applied to noisy rear-surface temperature data. To mimic the data arising from the laser flash experiment, we follow Carr [11] and add Gaussian noise to the sampled values from the previous section: $\tilde{T}_i = T_n(t_i) + z_i$, where z_i is a random number generated from a normal distribution with mean zero and standard deviation σ . Repeatedly generating synthetic rear-surface temperature rise datasets in this manner and calculating the corresponding thermal diffusivities allows distributions of the signed relative error to be constructed.

In Figure 2, results are reported for 10,000 realisations, low ($\sigma = 0.005$), moderate ($\sigma = 0.02$) and high ($\sigma = 0.05$) levels of noise, and the exponential pulse (22) with $\beta = 0.001 \text{ s}$ (as considered in the previous section). Example rear-surface temperature rise histories for each

level of noise are given in Figures 2(a)–(c). The relative error distributions in Figures 2(d)–(f) are smoothed using MATLAB’s inbuilt kernel smoothing function `ksdensity`. These figures also include the 0.5% and 99.5% quantiles for the data; for example, 99% of the estimates of α_2 have a relative error of between -1.61% and $+1.54\%$ for $\sigma = 0.02 \text{ }^\circ\text{C}$ (Figure 2e). Similar results are obtained for the rectangular and triangular pulses and are therefore not reported. Comparing Figures 2(e)–(f), we see that the thermal diffusivity estimates are slightly less accurate for the second layer than the first layer. This is because for this particular problem $\alpha_1 > \alpha_2$ (Table 1) so the small error incurred through approximating I_T via the trapezoidal rule (48) is amplified by a greater amount in Eq (45), where it is multiplied by α_1 , than in Eq (44), where it is multiplied by α_2 . Overall, the results in Figures 2(d)–(f) are comparable in accuracy to those reported previously for the rear-surface integral method [11].

Our numerical experiments so far have assumed that the laser pulse shape can be described exactly by either the rectangular (20), triangular (21) or exponential (22) pulse. We have also calculated the steady-state temperature, T_∞ , assuming known values for the amount of heat absorbed at the front surface, Q_∞ , and the volumetric heat capacity(s), ρc , $\rho_1 c_1$ and $\rho_2 c_2$ (i.e., by evaluating Eq (7) and Eq (31) directly using the parameter values in Table 1). We now explore calculating the thermal diffusivity directly using the discrete pulse shape measurements that

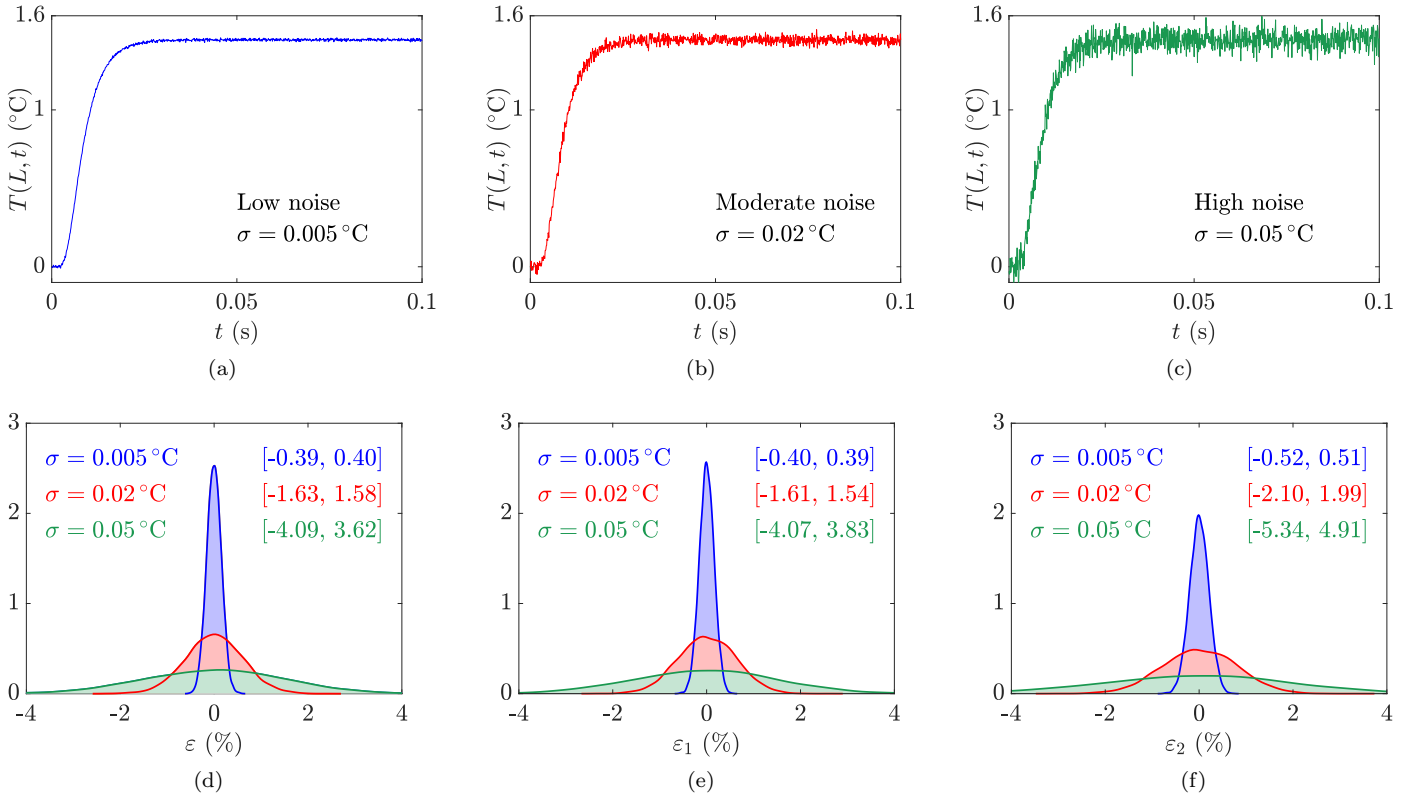


Figure 2: (a)–(c) Example realisations of the rear-surface temperature rise history using low, moderate and high levels of noise. (d)–(f) Signed relative error distributions for the thermal diffusivity estimates (d) α (17) (e) α_1 (44) and (f) α_2 (45) each implemented using the numerical approximation of I_T (48). Distributions and [0.5%,99.5%] quantile intervals are given for each of the three noise levels, with each distribution constructed using 10,000 realisations. All results are for the parameter values in Table 1 and the exponential pulse (22) with $\beta = 0.001$ s.

arise in a laser flash experiment and a value of T_{∞} inferred from the rear-surface temperature rise history (\tilde{T}_i where $i = 0, \dots, N$). Given discrete values of the heat pulse over time, $q(\hat{t}_j)$ where $\hat{t}_j = j\delta t/M$ and $j = 0, \dots, M$ (note that the time between pulse measurements δt differs from the time between rear-surface temperature rise measurements Δt), we approximate Q_{∞} using the trapezoidal rule:

$$Q_{\infty} \approx \frac{\delta t}{2} \sum_{j=1}^M [q(\hat{t}_{j-1}) + q(\hat{t}_j)], \quad (49)$$

and I_q using two applications of the trapezoidal rule

$$I_q \approx \Delta t \sum_{i=1}^N \left[1 - \frac{1}{Q_{\infty}} \left(\int_0^{\hat{t}_{i-1}} q(s) ds + \int_0^{\hat{t}_i} q(s) ds \right) \right], \quad (50)$$

$$\approx \Delta t \sum_{i=1}^N \left[1 - \frac{\delta t}{4Q_{\infty}} \left(\sum_{j=1}^{N_{i-1}} [q(\hat{t}_{j-1}) + q(\hat{t}_j)] + \sum_{j=1}^{N_i} [q(\hat{t}_{j-1}) + q(\hat{t}_j)] \right) \right], \quad (51)$$

where $N_i = t_i/\delta t$ is the number of intervals of length δt comprising the interval $[0, t_i]$ (i.e., the approximation of I_q assumes that $\Delta t/\delta t$ is an integer). To approximate T_{∞} from the rear-surface temperature rise history, we use the

height of the horizontal line of best fit through the last p measurements (Figure 3a), which yields the mean value

$$T_{\infty} \approx \frac{1}{p} \sum_{i=1}^p \tilde{T}_{N-p+i}. \quad (52)$$

Results in Figures 3(c)–(e) are given for the discrete heat pulse depicted in Figure 3(a), consisting of 201 discrete values between $t = 0$ and $t = 0.01$ s (inclusive) giving $M = 200$ and $\delta t = 5 \times 10^{-5}$ s in the approximations of Q_{∞} (49) and I_q (51). The discrete values are randomly generated by adding Gaussian noise of mean zero and standard deviation 40000 Jm^{-2} to the exponential pulse (22) with $\beta = 0.001$ s. Figure 3(b) provides an example realisation of the rear-surface temperature rise history for the homogeneous sample obtained by adding Gaussian noise to the solution of the heat flow model (3)–(5) with $q(t)$ defined as in Figure 3(a). The horizontal red dashed line in Figure 3(b) depicts the utilised approximation of T_{∞} (52) with $p = 200$. Comparing Figures 2(d)–(f) and Figures 3(c)–(e) we see that the approximations (49) and (51) roughly double the length of the [0.5%, 99.5%] quantile interval.

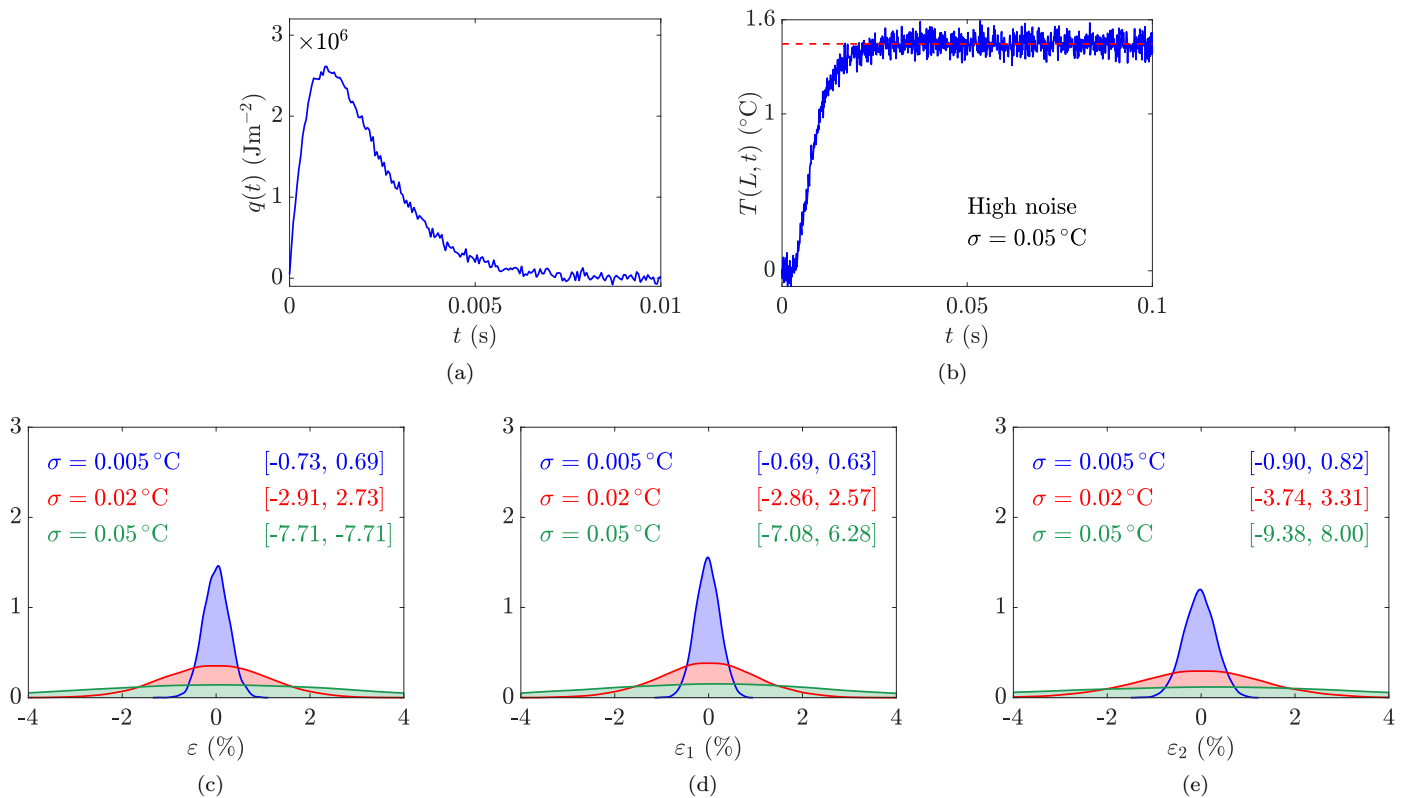


Figure 3: (c)–(e) Signed relative error distributions for the thermal diffusivity estimates (c) α (17) (d) α_1 (44) and (e) α_2 (45) each implemented using the numerical approximations of I_T (48) Q_∞ (49) and I_q (51). Distributions and [0.5%,99.5%] quantile intervals are given for each of the three noise levels, with each distribution constructed using 10,000 realisations; (b) provides an example realization. All results are for the parameter values in Table 1 and the noisy exponential pulse (22) with $\beta = 0.001$ s shown (a).

5. Conclusion

This paper has focussed on methods for calculating thermal diffusivity from laser flash experimental data. Specifically, we have shown how to account for real heat pulse shapes and two-layer samples using the recently-proposed rear-surface integral method [11]. The main contributions of the paper are new formulas for calculating the thermal diffusivity that correct for arbitrary heat pulse shapes:

- (i) Eqs (17)–(19) for calculating the thermal diffusivity of a homogeneous sample; and
- (ii) Eqs (44)–(47) for calculating the thermal diffusivity of one layer of a two-layer sample given the thermal diffusivity of the other layer.

Computational results confirmed the accuracy of the derived formulas and demonstrated how the formulas can be applied to the kinds of experimental data arising from the laser flash experiment.

The formulas derived in this paper are limited to thermally insulated samples, in which case the heat flow model reduces to a one-dimensional model in the direction of the thickness of the sample. Incorporating heat losses from the front and rear surfaces of the sample can be carried out

by combining the analysis in this paper with the discussion presented previously by Carr [11, Section 5]. Possible directions for future research also include extension of the rear-surface integral method to three-layer samples or two or three dimensional heat flow models; the latter of which could allow for heat losses from the other surfaces of the sample (Figure 1b–c) to be accounted for in the formulas.

The analysis presented in this paper can also be extended to other applications involving diffusion in homogeneous or layered materials in a straightforward manner. For example, by appropriately modifying the boundary and interface conditions (27)–(30), the rear-surface integral method can help parameterise a mathematical model of heat transfer through layered skin formulated by McInerney et al. [21].

Acknowledgements

This research was partially supported by the Australian Mathematical Sciences Institute (AMSI) who provided CJW with a 2018-2019 Vacation Research Scholarship.

Appendix A. Homogeneous finite volume scheme

In this appendix, we outline the finite volume scheme used to obtain a numerical solution to the homogeneous

heat flow model (3)–(5). We discretise the interval $[0, L]$ using a uniform grid consisting of n nodes such that the k th node is located at $x = kh =: x_k$, where $k = 1, \dots, n$ and $h = L/(n-1)$. The finite volume for an interior node ($k = 2, \dots, n-1$) extends from $x = x_k - h/2 =: x_k^w$ to $x = x_k + h/2 =: x_k^e$, the finite volume for the left boundary node ($k = 0$) extends from $x = 0 =: x_0^w$ to $x = h/2 =: x_1^e$ and the finite volume for the right boundary node ($k = n$) extends from $x = L - h/2 =: x_n^w$ to $x = L =: x_n^e$. Integrating the heat equation (3) over each finite volume yields:

$$V_k \frac{d}{dt} \left[\frac{1}{V_k} \int_{x_k^w}^{x_k^e} T(x, t) dx \right] = \alpha \frac{dT}{dx}(x_k^e, t) - \alpha \frac{dT}{dx}(x_k^w, t),$$

where $k = 1, \dots, n$ and $V_k = x_k^e - x_k^w$ is the length of the k th control volume. Let $T_k(t)$ denote the numerical approximation to $T(x, t)$ at $x = x_k$. Approximating the average of $T(x, t)$ over the k th control volume by T_k ; the spatial derivatives at $x = x_k^e$ ($k = 1, \dots, n-1$) and $x = x_k^w$ ($k = 2, \dots, n$) by second-order central difference approximations; and the spatial derivatives at $x = x_0^w = 0$ and $x = x_n^e = L$ using the boundary conditions (5) yields the semi-discretized system:

$$\frac{dT_k}{dt} = G_k, \quad k = 1, \dots, n,$$

with initial condition $T_k = 0$ at $t = 0$ (4) for $k = 1, \dots, n$ and right-hand side defined by

$$G_k = \begin{cases} \frac{2\alpha(T_{k+1} - T_k)}{h^2} + \frac{2q(t)}{h\rho c}, & k = 1, \\ \frac{\alpha(T_{k+1} - 2T_k + T_{k-1})}{h^2}, & k = 2, \dots, n-1, \\ \frac{2\alpha(T_{k-1} - T_k)}{h^2}, & k = n. \end{cases}$$

This initial value problem is solved using MATLAB 2017B's `ode15s` solver on the interval $[0, t_N]$ with specified absolute and relative tolerances (`AbsTol` and `RelTol`) of 10^{-12} and the interval of integration (`tspan`) specified to return the solution at $N+1$ equally-spaced discrete times: $t_i = i\Delta t$, where $i = 0, \dots, N$ and $\Delta t = t_N/N$. Using this solution, the rear-surface temperature rise history is given by the discrete values $T_n(t_0), \dots, T_n(t_N)$.

Appendix B. Two-layer finite volume scheme

In this appendix, we describe the finite volume scheme used to solve the two-layer heat flow model (23)–(30). We discretise the interval $[0, L]$ using a grid consisting of $n = n_1 + n_2 - 1$ nodes such that the k th node is located at $x = x_k$ with $x_k = (k-1)h_1$ for $k = 1, \dots, n_1$ and $x_k = \ell_1 + (k-n_1)h_2$ for $k = n_1+1, \dots, n_1+n_2-1$, where $h_1 = \ell_1/(n_1-1)$ and $h_2 = \ell_2/(n_2-1)$. Consider the finite volume for the interface node ($k = n_1$), which extends from $x = \ell_1 - h_1/2 =: x_{n_1}^w$ to $x = \ell_1 + h_1/2 =: x_{n_1}^e$. Integrating the heat equation in the first layer (23) from $x = x_{n_1}^w$ to $x = x_{n_1}$ and the heat

equation in the second layer (24) from $x = x_{n_1}$ to $x = x_{n_1}^e$ and adding the results yields:

$$\begin{aligned} \frac{d}{dt} \left[\rho_1 c_1 \int_{x_{n_1}^w}^{x_{n_1}^e} T_1(x, t) dx + \rho_2 c_2 \int_{x_{n_1}}^{x_{n_1}^e} T_2(x, t) dx \right] \\ = k_2 \frac{dT_2}{dx}(x_{n_1}^e, t) - k_1 \frac{dT_1}{dx}(x_{n_1}^w, t) \\ + k_1 \frac{dT_1}{dx}(x_{n_1}, t) - k_2 \frac{dT_2}{dx}(x_{n_1}, t), \end{aligned} \quad (\text{B.1})$$

for $k = n_1$. Let $T_{n_1}(t)$ denote the numerical approximation to $T_1(x, t)$ and $T_2(x, t)$ at $x = x_{n_1} = \ell_1$, which are both equal due to the continuity of temperature imposed at the interface (29). Approximating the first integral on the left-hand side of Eq (B.1) by a right-hand quadrature rule and the second integral by a left-hand quadrature rule, and using the continuity of the flux (30) on the right-hand side of Eq (B.1) yields the semi-discretised equation for the interface node. The boundary nodes and the nodes interior to the first and second layers are handled in an identical manner to that discussed previously for the single-layer finite volume scheme (Appendix A). In summary, the semi-discretised system for the two-layer heat flow model (23)–(30) is given by:

$$\frac{dT_k}{dt} = G_k, \quad k = 1, \dots, n_1 + n_1 - 1,$$

with initial condition $T_k = 0$ at $t = 0$ (25)–(26) for $k = 1, \dots, n_1 + n_1 - 1$ and right-hand side defined by

$$G_k = \begin{cases} \frac{2\alpha_1(T_2 - T_1)}{h_1^2} + \frac{2q(t)}{h_1 \rho_1 c_1}, & k = 1, \\ \frac{\alpha_1(T_{k+1} - 2T_k + T_{k-1})}{h_1^2}, & k = 2, \dots, n_1 - 1, \\ \frac{2 \left[\frac{k_2}{h_2} T_{k+1} - \left(\frac{k_1}{h_1} + \frac{k_2}{h_2} \right) T_k + \frac{k_1}{h_1} T_{k-1} \right]}{\rho_1 c_1 h_1 + \rho_2 c_2 h_2}, & k = n_1, \\ \frac{\alpha_2(T_{k+1} - 2T_k + T_{k-1})}{h_2^2}, & k = n_1 + 1, \dots, n_1 + n_2 - 2, \\ \frac{2\alpha_2(T_{k-1} - T_k)}{h_2^2}, & k = n_1 + n_2 - 1. \end{cases}$$

This initial value problem is then solved to obtain the rear-surface temperature rise history in an identical manner to that described for the homogeneous case at the end of Appendix A.

References

- [1] J. Blumm, J. Opfermann, Improvement of the mathematical modelling of flash measurements, *High Temp.-High Press.* 34 (2002) 515–521.
- [2] B. Czél, K. A. Woodbury, J. Woolley, G. Gróf, Analysis of parameter estimation possibilities of the thermal contact resistance using the laser flash method with two-layer specimens, *Int. J. Thermophys.* 34 (2013) 1993–2008.
- [3] L. Vozár, W. Hohenauer, Flash method of measuring the thermal diffusivity. A review, *High Temp.-High Press.* 35–36 (2003) 253–264.

- [4] W. J. Parker, R. J. Jenkins, C. P. Butler, G. L. Abbott, Flash method of determining thermal diffusivity, heat capacity, and thermal conductivity, *J. Appl. Phys.* 32 (1961) 1679–1684.
- [5] D. Jeon, S. H. Kim, W. Choi, C. Byon, An experimental study on the thermal performance of cellulose-graphene-based thermal interface materials, *Int. J. Heat Mass Tran.* 132 (2019) 944–951.
- [6] C. Wang, S. Zhang, L. Guo, Investigation on the effective thermal conductivity of typical pidgeon process briquette with a combined model, *Int. J. Heat Mass Tran.* 115 (2017) 1348–1358.
- [7] J. Zajas, P. Heiselberg, Determination of the local thermal conductivity of functionally graded materials by a laser flash method, *Int. J. Heat Mass Tran.* 60 (2013) 542–548.
- [8] Y.-H. Zhao, Z.-K. Wu, S.-L. Bai, Thermal resistance measurement of 3D graphene foam/polymer composite by laser flash analysis, *Int. J. Heat Mass Tran.* 101 (2016) 470–475.
- [9] R. C. Heckman, Finite pulse-time and heat-loss effects in pulse thermal diffusivity measurements, *J. Appl. Phys.* 44 (1973) 1455–1460.
- [10] J. A. Cape, G. W. Lehman, Temperature and finite pulse-time effects in the flash method for measuring thermal diffusivity, *J. Appl. Phys.* 34 (1963) 1909–1913.
- [11] E. J. Carr, Rear-surface integral method for calculating thermal diffusivity from laser flash experiments, *Chem. Eng. Sci.* 199 (2019) 546–551.
- [12] T. Azumi, Y. Takahashi, Novel finite pulse-wide correction in flash thermal diffusivity measurement, *Rev. Sci. Instrum.* 52 (1981) 1411–1413.
- [13] K. B. Larson, K. Koyama, Measurement by the flash method of thermal diffusivity, heat capacity, and thermal conductivity in two-layer composite samples, *J. Appl. Phys.* 39 (1968) 4408.
- [14] H. M. James, Some extensions of the flash method of measuring thermal diffusivity, *J. Appl. Phys.* 51 (1980) 4666–4672.
- [15] H. J. Lee, Thermal Diffusivity in Layered and Dispersed Composites, Ph.D. thesis, Purdue University, Lafayette, IN, USA., 1975.
- [16] J. A. Koski, Thermal diffusivity measurements of molten salts using a three-layered cell by the laser flash method, *Rev. Sci. Instrum.* 61 (1990) 2645–2649.
- [17] J. A. Koski, Sensitivity and accuracy analysis of pulse diffusivity measurements on layered samples, *Thermal Conductivity* 18 (1985) 525–536.
- [18] L. Chen, A. M. Limarga, D. R. Clarke, A new data reduction method for pulse diffusivity measurements on coated samples, *Comp. Mater. Sci* 50 (2010) 77–82.
- [19] E. J. Carr, Calculating how long it takes for a diffusion process to effectively reach steady state without computing the transient solution, *Phys. Rev. E* 96 (2017) 012116.
- [20] E. J. Carr, M. J. Simpson, Accurate and efficient calculation of response times for groundwater flow, *J. Hydrol.* 558 (2018) 470–481.
- [21] S. McNerney, E. J. Carr, M. J. Simpson, Parameterising continuum models of heat transfer in heterogeneous living skin using experimental data, *Int. J. Heat Mass Tran.* 128 (2019) 964–975.